

Highly luminous supernovae associated with gamma-ray bursts

II. The luminous blue bump in the afterglow of GRB 140506A

D. A. Kann^{*1,2}, A. Rossi^{**3}, S. R. Oates⁴, S. Klose⁵, M. Blazek⁶, J. F. Agüí Fernández^{2,6}, A. de Ugarte Postigo^{7,8},
C. C. Thöne⁹, and S. Schulze¹⁰

¹ Hessian Research Cluster ELEMENTS, Giersch Science Center, Max-von-Laue-Straße 12, Goethe University Frankfurt, Campus Riedberg, D-60438 Frankfurt am Main, Germany

² Instituto de Astrofísica de Andalucía (IAA-CSIC), Glorieta de la Astronomía s/n, 18008 Granada, Spain

³ INAF - Osservatorio di Astrofisica e Scienza dello Spazio, via Piero Gobetti 93/3, 40129 Bologna, Italy

⁴ Department of Physics, Lancaster University, Lanes LA1 4YB, UK

⁵ Thüringer Landessternwarte Tautenburg, Sternwarte 5, 07778 Tautenburg, Germany

⁶ Centro Astronómico Hispano en Andalucía, Observatorio de Calar Alto, Sierra de los Filabres, 04550 Gérgal, Almería, Spain

⁷ Artemis, Université de la Côte d'Azur, Observatoire de la Côte d'Azur, CNRS, 06304 Nice, France

⁸ Aix Marseille Univ, CNRS, LAM Marseille, France

⁹ Astronomical Institute, Czech Academy of Sciences, Fričova 298, Ondřejov, Czech Republic

¹⁰ Center for Interdisciplinary Exploration and Research in Astrophysics (CIERA), Northwestern University, 1800 Sherman Ave., Evanston, IL 60201, USA

Received 30 September 2021 / Accepted 30 January 2024

ABSTRACT

Context. The supernovae (SNe) associated with gamma-ray bursts (GRBs) are generally seen as a homogeneous population, but at least one exception exists: the highly luminous SN 2011kl associated with the ultra-long GRB 111209A. Such outliers may also exist for more typical GRBs.

Aims. Within the context of a systematic analysis of photometric signatures of GRB-associated SNe, we found an anomalous bump in the late-time transient following GRB 140506A at redshift $z=0.889$. We hereby aim to show this bump is significantly more luminous and blue than usual SNe following GRBs.

Methods. We compiled all available data from the literature and added a full analysis of the *Swift*/UVOT data, which allowed us to trace the light curve from the first minutes all the way to the host galaxy and to construct a broad spectral energy distribution (SED) of the afterglow that extends the previous SED analysis based on ground-based spectroscopy.

Results. We find robust evidence of a late-time bump following the afterglow that shows evidence of a strong color change, with the spectral slope becoming flatter in the blue region of the spectrum. This bump can be interpreted as a luminous SN bump that is spectrally dissimilar to typical GRB-SNe. Correcting it for the large line-of-sight extinction makes the SN associated with GRB 140506A the most luminous detected so far. Even so, it would be in agreement with a luminosity-duration relation of GRB-SNe.

Conclusions. While not supported by spectroscopic evidence, it is likely the bump following GRB 140506A is the signature of an SN that is spectrally dissimilar to classical GRB-SNe and more similar to SN 2011kl – while being associated with an average GRB, indicating the GRB-SN population is more diverse than previously thought and can reach luminosities comparable to those of superluminous SNe.

Key words. Gamma-Ray Bursts: Individual: GRB 140506A

1. Introduction

The link between “long gamma-ray bursts” (GRBs) usually exhibiting a duration of > 2 s (however, see Ahumada et al. 2021; Zhang et al. 2021; Rossi et al. 2022), also labeled “Type II GRBs” in a more physically motivated, duration-independent classification scheme (Zhang et al. 2009; Kann et al. 2011), and the explosive deaths of massive stars has now been firmly established (see Woosley & Bloom 2006; Cano et al. 2017 for reviews). Beginning with the prototypical, well-studied supernova (SN) 1998bw associated with the low-luminosity, nearby GRB 980425 (Galama et al. 1998; Clocchiatti et al. 2011), all GRB-SNe that have been studied well have been found to be explosions of highly stripped stars (so-called broad-lined Type Ic

SNe), which are missing signatures of hydrogen and helium in their spectra. Perhaps surprisingly, these SNe have been shown to be very similar in terms of luminosity, ejecta and nickel masses, and energy release (Melandri et al. 2014), whether they have been associated with a spectrally soft, low-luminosity X-ray flash such as XRF 060218 (e.g. Pian et al. 2006; Mazzali et al. 2006), a moderately soft and energetic GRB such as GRB 030329 (e.g. Hjorth et al. 2003; Matheson et al. 2003; Stanek et al. 2003), or a highly luminous and spectrally hard “true cosmological” GRB such as GRB 130427A (Xu et al. 2013; Melandri et al. 2014).

A decade ago, a startling outlier was discovered. GRB 111209A was a GRB of extreme duration in gamma-rays (Golenetskii et al. 2011; Gendre et al. 2013; Stratta et al. 2013), leading, together with the “Christmas Burst” GRB 101225A (Thöne et al. 2011), to the establishment of the ultra-long-

* Deceased

** E-mail: andrea.rossi@inaf.it

duration GRB class (Levan et al. 2014). GRB 111209A was found to be associated with a well-detected SN, SN 2011kl, which exhibited properties very different from usual GRB-SNe, being both more luminous, bluer, and spectrally dissimilar to typical Type Ic GRB-SNe, and closer in resemblance, spectroscopically, to superluminous SNe (SLSNe Greiner et al. 2015; Mazzali et al. 2016). Notwithstanding its extreme duration, both GRB 111209A and its afterglow are not unprecedented (Kann et al. 2018), but a detailed study shows SN 2011kl differing from GRB-SNe in many aspects (Kann et al. 2019).

This discovery immediately opened multiple new lines of inquiry. We now question whether all ultra-long GRBs are associated with anomalous GRB-SNe, and if so, whether they are similar to SN 2011kl or outliers in other aspects. Moreover, we would like to know if such peculiar, highly luminous GRB-SNe are exclusively associated with ultra-long GRBs or if they can also occur following “standard” GRBs.

So far, the lack of more detailed studies of ultra-long GRBs (which are very rare) has prevented us from exploring the first question further. However, here we present evidence of a highly luminous GRB-SN associated with a “standard” GRB, which indicates that these events are not limited to ultra-long GRBs. In the context of a systematic study of late-time emission in GRB afterglows at $z \lesssim 1$, we find that the per se unremarkable (at high energies) GRB 140506A, which has been studied in detail stemming from its peculiar line-of-sight in terms of extinction and spectral features (Fynbo et al. 2014; Heintz et al. 2017), exhibits a bump at late times that shows a strong color change from very red to very blue. This bump is significantly brighter than the final host-galaxy magnitudes, making the interpretation as a late-time SN component compelling. Furthermore, we analyzed spectral energy distribution (SED) of the afterglow, determined the dust extinction along the line of sight, and placed the potential SN in a larger context of extinction-corrected GRB-SNe.

The paper is organized as follows. In Sect. 2, we present GRB 140506A and our observations of the afterglow. We discuss our analysis and our results in Sect. 3, and we place the event in context in Sect. 4 before concluding in Sect. 5.

In our calculations, we assume a flat Universe with a matter density $\Omega_M = 0.27$, a cosmological constant $\Omega_\Lambda = 0.73$, and a Hubble constant $H_0 = 71 \text{ km s}^{-1} \text{ Mpc}^{-1}$ (Spergel et al. 2003), to remain in agreement with our older sample papers. Errors are given at the 1σ level, and upper limits are given at the 3σ level for a parameter of interest. For temporal and spectral power laws, we assume $F(t, \nu) \propto t^{-\alpha} \nu^{-\beta}$; therefore, temporally decaying light curves and spectra rising in brightness toward the red (the typical situation for GRB afterglows) have positive α and β values.

2. Observations of GRB 140506A

2.1. Prompt emission phase

GRB 140506A triggered the *Neil Gehrels Swift Observatory* (*Swift* hereafter, Gehrels et al. 2004) at 21:07:36 UT on 6 May, 2014 (Gompertz et al. 2014). The satellite slewed immediately, localizing the event precisely with X-ray, ultra-violet (UV), and optical detections. It was a moderately bright GRB consisting of an initial spike followed by several fainter emission episodes, and it also triggered *Fermi*/GBM (Jenke 2014) and *Konus-Wind* (Golenetskii et al. 2014). The T_{90} ¹ derived by *Swift* was

¹ The time span over which 90% of the integrated counts are emitted, beginning 5% after the start of detection and ending at 95%. This is a general duration measure used for GRBs.

$111.1 \pm 9.6 \text{ s}$ (Markwardt et al. 2014), so clearly not of ultra-long duration². Tsvetkova et al. (2017) reported a detailed analysis of the *Konus-Wind* detection of GRB 140506A, deriving a fluence in the 10 – 10000 keV energy band of $5.74^{+0.52}_{-0.34} \times 10^{-6} \text{ erg cm}^{-2}$, and a spectrum that is best fit by a cut-off power law with $\alpha_{\text{prompt}} = 1.32^{+0.23}_{-0.26}$ and $E_{\text{peak}} = 200^{+90}_{-42} \text{ keV}$. Using these parameters and the redshift $z = 0.88911$ (Fynbo et al. 2014), we deduce (following Agüí Fernández et al. 2023) an isotropic energy release in the rest-frame 1 keV to 100 MeV band of $\log E_{\text{iso}}/\text{erg} = 52.15 \pm 0.03$, implying GRB 140506A is an average GRB that is neither particularly sub- nor super-luminous.

Nonetheless, the GRB features one interesting aspect, namely a peculiar, red, and strongly curved afterglow spectrum, leading to a detailed spectroscopic and photometric analysis by Fynbo et al. (2014), which was followed by a host-galaxy study (Heintz et al. 2017). In the late-time data presented in Fynbo et al. (2014), the afterglow decay flattened considerably, seemingly implying the host-galaxy level had been reached; however, Heintz et al. (2017) showed this to be incorrect, finding further significant decay between ≈ 2 months and a year post-burst. They even remarked that the earlier plateau phase is similar to what one would expect from a GRB-SN, but they did not pursue the topic further.

2.2. Follow-up observations

Fynbo et al. (2014) presented ground-based photometric observations starting 0.33 d after the GRB, with detections spanning from the GROND g' band to the GROND K_s band. Their last detection epoch is 68 d post-burst. They also obtained *Very Large Telescope* X-shooter spectra at 8.8 and 33 h after the burst and a spectrum at 52 days using the *Magellan* telescope. Heintz et al. (2017) added host-galaxy data spanning from u' to the *Spitzer* IRAC1 band (at $3.6 \mu\text{m}$) taken about a year after the GRB, when any transient is expected to have faded.

To expand this data set both temporally and spectrally, we analyzed the *Swift* UltraViolet-Optical Telescope (UVOT, Roming et al. 2005) data. UVOT began settled observations of the field of GRB 140506A 108 s after the *Swift* Burst Alert Telescope (BAT) trigger, with initial results reported in Siegel & Gompertz (2014). The data (in AB mags) are given in Table A.1. The last low-significance detection is at 1.8 d, with upper limits until 30 d. We note that Fynbo et al. (2014) also analyzed the UVOT data and only claimed detections for *ubv white*, with a low-S/N detection in *uvw1*. While the S/N is certainly low ($< 2\sigma$), we also report multiple early detections in *uvm2* and *uvw2*.

Before extracting count rates from the event lists, the astrometry was refined following the methodology of Oates et al. (2009). The source counts were initially extracted using a source region with a $5''$ radius. When the count rate dropped to below 0.5 counts per second, we used a source region with a $3''$ radius. In order to be consistent with the UVOT calibration, these count rates were then corrected to $5''$ using the curve of growth contained in the calibration files. Background counts were extracted using three circular regions with radii of $10''$ located in source-free regions. The count rates were obtained from the event and image lists using the *Swift* tools *uvotevt1c* and *uvotsource*, respectively. They were converted to magnitudes using the UVOT photometric zero points (Poole et al. 2008; Breeveld et al. 2011). To improve the signal-to-noise ratio (S/N), the count rates in each filter were binned using $\Delta t/t = 0.1$, leading to longer but deeper exposures at later times. The early event-

² T_{90} from *Konus-Wind* and *Fermi*/GBM are about half this value.

mode *white* and *u* finding-charts were bright enough to be split into multiple exposures.

3. Results

3.1. The afterglow

The multicolor light curve of the optical transient (OT) that followed GRB 140506A is shown in Fig. 1. UVOT data are presented in Table A.1. We did not add UVOT upper limits for the sake of legibility, and near-infrared (NIR) *JHK_s*-band data (from Fynbo et al. 2014) as they do not contribute notably to the light-curve fit. They are used in the SED, however (Sect. 3.3). The early UVOT data, despite showing (for the most part) low S/N detections with large errors, agree well with a single power-law fit over all bands and the complete time span. The one exception is the first two data points derived from the *u* event-mode finding-chart at $\approx 340 - 370$ s; these lie $\sim 3\sigma$ above the rest of the *u*-band data. The *Swift*/X-ray telescope (XRT, Burrows et al. 2005) data at this time, as given³ on the XRT repository (Evans et al. 2007, 2009), indeed show a strong flare taking place right at this time, linking the elevated emission to an additional component, likely stemming from internal shocks. However, an even more powerful earlier X-ray flare, peaking at ≈ 120 s, is not visible in the time-resolved *white* finding chart (Fig. 1). We find that the entire UVOT data are well-fit ($\chi^2/\text{d.o.f.} = 0.65$) by a simultaneous, multiband, single-power-law fit with decay of $\alpha_1 = 0.90 \pm 0.03$. This assumes that the evolution of the afterglow is achromatic. While the early time prompt-emission flare may have a different SED, it only affects two data points, and the X-ray light curve shows no further evidence of flaring. The fit equation determines the afterglow magnitude in each band (all data have been corrected for Galactic extinction following Schlafly & Finkbeiner 2011), which yields the UVOT-data SED.

The reddened and relatively faint afterglow implies that it is hardly detected beyond ≈ 0.14 d, and therefore there is no useful overlap with the ground-based data set from Fynbo et al. (2014). We therefore fit that data independently. It clearly shows a shallower decay than before, which is an unusual but not unprecedented phenomenon. The data extending from 0.33 to 3.5 days were again fit by single decay for which we find $\alpha_2 = 0.54 \pm 0.03$. A large data gap follows and then two further epochs (as well as a single unfiltered point, calibrated to *r'*, in-between) at 21 and 68 days (as well as the host-galaxy observations about a year after the GRB). A simple extrapolation of the $\alpha_2 = 0.54$ decay showed that at 21 days, the fit strongly overestimated the actual data; therefore, a break must have occurred, likely a jet break. However, as the following plateau is clearly not the host-galaxy level, this would imply either a strong, long-lasting flattening of the afterglow, which is very unlikely, or a new emission component.

3.2. The supernova

Despite the high redshift and the large line-of-sight extinction in the GRB host galaxy, the most natural explanation for the observed re-brightening of the light curve in the optical bands is an SN following GRB 140506A, as Heintz et al. (2017) already speculated.

The SN components associated with GRBs were first studied systematically by Zeh et al. (2004), who introduced the k, s context as described below. Based on the detailed light curves of the

Table 1. SED fit results for OT that followed GRB 140506A.

| β | A_V (mag) | dust model | $\chi^2/\text{d.o.f.}$ |
|-----------------|-----------------|------------|------------------------|
| 1.79 ± 0.07 | — | N/A | 6.09 |
| 0.24 ± 0.27 | 1.12 ± 0.18 | MW | 1.04 |
| 0.25 ± 0.36 | 1.50 ± 0.25 | LMC | 1.65 |
| 0.23 ± 0.34 | 1.11 ± 0.22 | SMC | 4.21 |

prototypical GRB-SN 1998bw at $z=0.0085$ (Galama et al. 1998; Clocchiatti et al. 2011), and assuming that the general shape of GRB-SN light curves is identical, templates of SN 1998bw can be created at other redshifts. These templates can then be altered based on the luminosity factor k , with $k = 1$ implying the GRB-SN is just as luminous as SN 1998bw would be at the specific GRB redshift in the specific rest-frame band corresponding to the observer-frame band the measurements were taken in. Furthermore, without changing its fundamental shape, the light curve's temporal evolution can be compressed ($s < 1$) or stretched ($s > 1$) with the stretch factor, s . This model fits almost all GRB-SN light curves very well, and in particular that of SN 2011kl, despite it being over-luminous compared to SN 1998bw (Kann et al. 2019).

We derived template light curves for SN 1998bw at the redshift of GRB 140506A, $z = 0.88911$. At this redshift, the observer-frame $g'r'i'z'$ bands lie between *uv*m2 and *uv*w1, between *uv*w1 and *U*, between *U* and *B*, and at about g' in the rest frame, respectively. SN 1998bw was observed densely in *BVR_CI_C* and with less follow-up in *U*. To emulate bands that lie blueward of *U* in the rest frame, a simple power law with $F(\nu) \propto \nu^{-3}$ was assumed (Zeh et al. 2004). Therefore, we caution here that results derived from the g' band come with a caveat of uncertainty. As the data are sparse, with only r' having three data points during the SN-dominated epochs, we fixed s to be a shared parameter between bands, and then we performed a simultaneous afterglow+SN+host fit, where the afterglow evolved achromatically but the SN can have different k values for each band, and the host-galaxy magnitudes were also individual for each band (for z' , we estimated a host magnitude $z' = 24.0$ mag based on the SED plot of Heintz et al. 2017).

The large data gap from three to 21 days implies that the break time and post-break decay slope are degenerate and, therefore, could not both be left as free parameters in the fit. However, the X-ray light curve deviates downward at $\approx 6 - 7$ days, which would favor an early and achromatic break time. Therefore, in the following we assume the break to be at 7 d. The fit is good ($\chi^2/\text{d.o.f.} = 0.76$), and the resulting k, s factors are shown in Table 2. The fit is shown in Fig. 1.

3.3. Spectral energy distribution

The equation used to fit the afterglow+SN+host uses overlapping components; therefore, the normalizations that define the afterglow magnitudes at 1 / 7 d are pure afterglow values and directly represent the SEDs at these times. The afterglow fits are achromatic, implying that these SEDs are valid over the fitting epochs. However, as stated, the UVOT and ground-based data overlap only marginally. We thus produced two SEDs. However, still assuming the underlying spectrum remains constant, we could fit the two SEDs simultaneously, sharing the intrinsic spectral slope and the extinction, but allowing the normalization of the two SEDs to vary independently.

³ https://www.swift.ac.uk/xrt_curves/00598284/

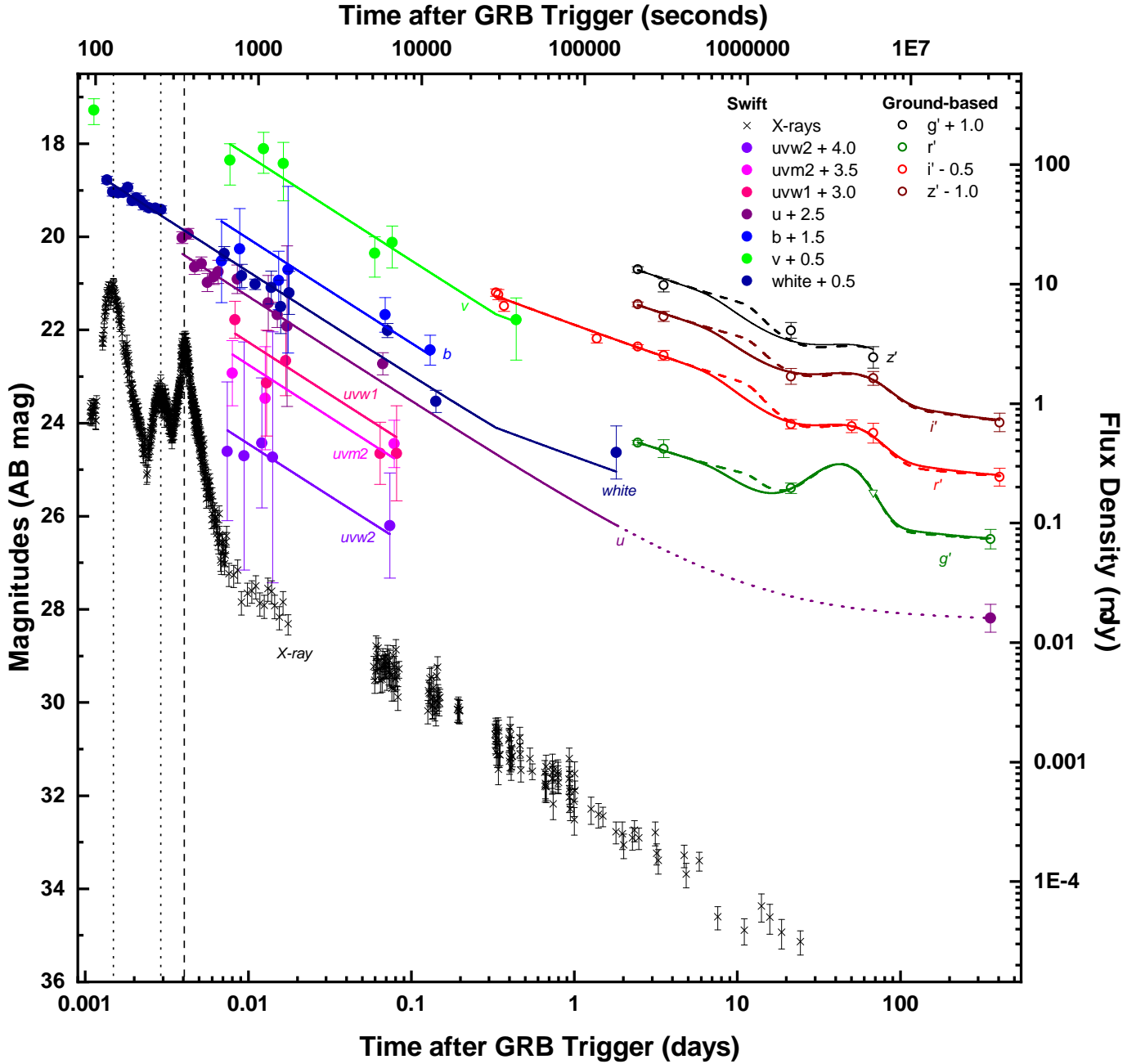


Fig. 1. Observations of optical transient that followed GRB 140506A. UVOT data (*uvw2*, *uvm2*, *uvw1*, *u*, *b*, *v*, *white*) are presented in this paper (Table A.1). Ground-based *u'g'r'i'z'* magnitudes are from Fynbo et al. (2014) and Heintz et al. (2017). The downward-pointing triangle in *g'* at 68 days is an upper limit. We do not show UVOT upper limits and *JHK_s* data as they add no relevant information. Data are corrected for Galactic extinction, given in the AB magnitude system, and additionally offset by the values given in the legend to improve legibility. The flux density scale is only valid for the (unshifted) *r'* band. The rest was shifted for clarity. The scale of the X-ray data was chosen arbitrarily. We show two possible fits with breaks at 7 (solid fit curve) and at 12 (dotted fit curve) days, which include both the afterglow and the SN/host contributions. Dotted vertical lines mark the peaks of two early X-ray flares that have no counterparts in the UV/optical range, whereas the flare marked by the dashed vertical line is also detected by UVOT. The flatter decay after 0.33 d in the late UVOT *v* and *white* light curves is simply the shifted *r'*-band fit (see text for more details).

The result is shown in Fig. 2, and values are given in Table 1. A fit without dust results in a very red slope and a bad fit. Fits with dust (based on Pei 1992) improve the fit significantly, but the shape of the double SED is not simple. The usual dust that fits GRB afterglows well, that of the Small Magellanic Cloud (SMC), also manages to fit the ground-based SED quite well, but it fails to fit the UVOT SED, strongly underestimating the UV emission. The dust of the Large Magellanic Cloud

(LMC) represents a strong improvement, but it results in a negative spectral slope, which is very unlikely. The best fit is given by using Milky Way (MW) dust with a strong 2175 Å bump but shallow UV slope, only this dust type is capable of modeling the whole double SED adequately. Intriguingly, the derived values are very similar to those from the SMC dust fit (Table 1), but the MW model agrees fully with the data. An upturn in the bluest

Table 2. Fit results for GRB 140506A supernova component.

| Fit model | s | k (fitted) | k (extinction-corrected) |
|-------------|-----------------|--------------------------|----------------------------|
| 7 day break | 1.96 ± 0.11 | $k_{g'} = 5.45 \pm 1.21$ | $k_{g'} = 76.96 \pm 17.22$ |
| | | $k_{r'} = 1.19 \pm 0.39$ | $k_{r'} = 6.65 \pm 2.33$ |
| | | $k_{i'} = 1.20 \pm 0.39$ | $k_{i'} = 4.95 \pm 1.75$ |
| | | $k_{z'} = 1.00 \pm 0.41$ | $k_{z'} = 3.32 \pm 1.45$ |

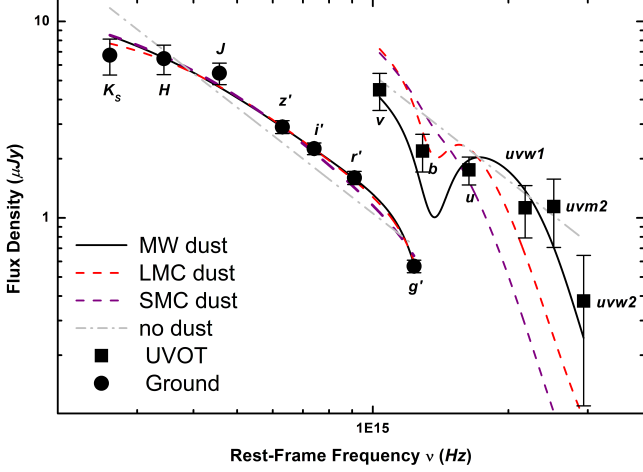


Fig. 2. SED of the OT that followed GRB 140506A. The SED in the v -to- $uvw2$ filter bands was derived from UVOT data at 24 h post-burst. The one covering the K_s -to- g' filters is based on ground-based data at 7 d after the GRB. We show fits with no dust (gray dash-dot-dotted line), Milky Way dust (black compact line), Large Magellanic Cloud dust (red dashed line), and Small Magellanic Cloud dust (violet dashed line). The Milky Way dust fit is the best (see text for more details).

region of the X-shooter spectrum is also reported by Fynbo et al. (2014) as would be expected from a MW dust extinction model (however, see Heintz et al. 2017). Such a high extinction value is similar to several other sightlines featuring a 2175 Å bump, such as those toward GRB 070802 (Krühler et al. 2008; Elíasdóttir et al. 2009; Kann et al. 2010; Zafar et al. 2012), GRB 120119A (Morgan et al. 2014, Kann et al., in prep.), GRB 180325A (Zafar et al. 2018a, Kann et al., in prep.), and GRB 190114C (Thöne et al., in prep.).

Fynbo et al. (2014) reported an intrinsic spectral slope of the late (post-prompt emission flares) X-ray spectrum of $\beta_X = 0.75 \pm 0.07$. This is a hard spectrum already, but assuming a cooling break between X-rays and optical implies $\beta_{\text{opt}} = 0.25$, which is in excellent agreement with our result. Fynbo et al. (2014) also verified that the cooling break lies between the X-ray and optical band. For such a spectrum and the parametrization of Fitzpatrick & Massa (2007), Fynbo et al. (2014) found $A_V = 0.9$ mag, which is close to our result. Furthermore, they reported that their spectrum cannot be fit with an MW extinction law; however, they simply assumed $A_V = 0.8$ mag, which is significantly lower than the value we derive. We independently analyzed the X-ray-to-optical SED and confirm the X-ray results of Fynbo et al. (2014), with a cooling break lying in the extreme UV. A fit purely with X-ray and UVOT data also finds results in agreement with the UV-optical-NIR-only fits within errors.

Heintz et al. (2017) presented strongly binned spectra from the first two X-shooter epochs (Fynbo et al. 2014). They found that a subtraction of their X-shooter host-galaxy spectrum (taken

over a year after the GRB, so there is no longer any SN contribution) essentially removes all flux at wavelengths < 4000 Å; that is, the upturn seen in the X-shooter afterglow spectra at bluest wavelengths was mostly pure host contribution. They used this as evidence to rule out the “extreme 2175 Å bump” model and derive a dust extinction model with an extremely strong UV extinction. However, this is in contrast with our clear UVOT u detection and our UVOT-based SED, which shows a relatively flat $b - u$ color that agrees with the existence of a 2175 Å bump, as well as the lower S/N detection in the UVOT lenticular filters, which should all be extremely damped if the Heintz et al. (2017) dust model is correct. Additionally, from the GROND SED, we do not detect a strong downturn yet in the observer-frame r' band, bluer than the < 8000 Å downturn Fynbo et al. (2014) and Heintz et al. (2017) derive from their X-shooter spectra. We do not readily have a solution for this conundrum.

Independent of whether the extinction curve is an extreme 2175 Å bump model as suggested by Fynbo et al. (2014) or the extreme UV extinction model presented by Heintz et al. (2017), the SN results we report in Sect. 3.2 are robust. The extinction Fynbo et al. (2014) found is similar to our result, and the model of Heintz et al. (2017) also leads to a strong correction for extinction, they find $A_V = 1.04$ mag, which is even closer to our result. Furthermore, for the SN, only the $g'r'i'z'$ data are important, and the two extinction models are similar in this observer-frame wavelength range.

From our SED fit, we derive host-galaxy extinction correction factors of $F_{\text{corr},g'} = 14.1 \pm 2.2$, $F_{\text{corr},r'} = 5.6 \pm 0.9$, $F_{\text{corr},i'} = 4.1 \pm 0.6$, and $F_{\text{corr},z'} = 3.3 \pm 0.5$. Using these corrections and applying the standard procedure for error propagation, we achieve the final values given in the last column of Table 2.

4. Discussion

Tables 2 and 3 show that despite the relatively large difference in the chosen break time, the derived values are very similar to each other, and the break time (within reasonable limits) has only a minor influence on the SN. The second aspect is that the resulting values are large. Generally, detecting an SN component at a redshift of ≈ 0.9 is not expected and needs either a bright SN or a very faint host galaxy. The contrast between the SN component and the moderately bright host is immediately visible (Heintz et al. 2017), implying a luminous SN.

4.1. Light-curve break time

In Sect. 3.1 we show how we found that a break in the optical light curve must exist between about three and 20 days; otherwise, at 21 days the fit strongly overestimates the observed flux. Motivated by the observed shape of the *Swift*/XRT light curve, we adopted a break time of 7 d. To study how the choice of the break time affects the evidence for an underlying SN component, we also modeled the optical light curve with a break at 12

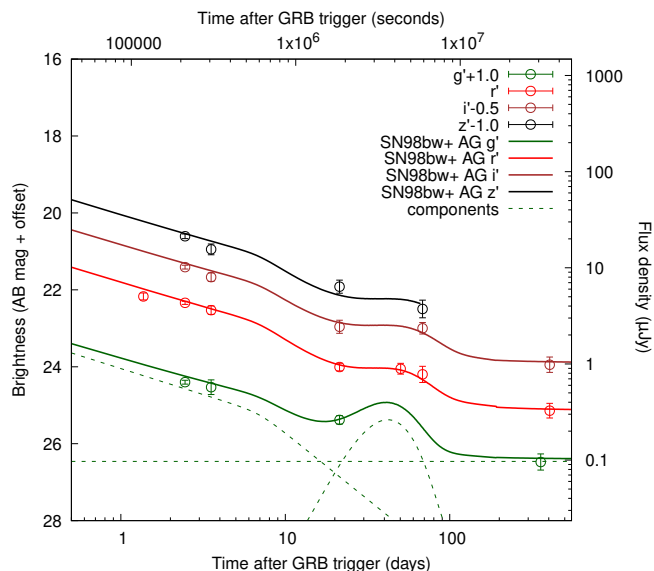


Fig. 3. Late $g'r'i'z'$ light curves of OT. For the g' band, we also show its breakdown into afterglow, host-galaxy, and SN flux. Data are corrected for Galactic extinction, given in the AB magnitude system, and additionally offset by the values given in the legend, but they are not corrected for the extinction in the host, as in Fig. 1. For the SN component, we used the best-fit values provided in Table 2.

d. These two choices lead to two very different results for the post-break decay slope: $\alpha_3 = 1.38 \pm 0.22$ for a break at seven days, and $\alpha_3 = 2.25 \pm 0.42$ for a break at 12 days. The resulting fits are indistinguishable in quality, and indeed, for both cases we obtain $\chi^2/\text{d.o.f.} = 0.76$ (Fig. 1).⁴ The SN component is essentially unaffected in shape by the choice of the break time (but not in intrinsic luminosity). Of course, these two choices do not map out the complete possible parameter region. For example, a break at 7 d (or even earlier) followed by a steep decay > 2 is also possible, which would make the SN even more luminous. A late break with a shallow post-break decay would be in disagreement with the data at 21 days, however.

In conclusion, a later break time results in a more luminous SN. However, the size of this effect is small (Table 3). Therefore, given that the derived luminosity of the SN does only marginally depend on the adopted break time, in the following we continue assuming a break at 7 d. Finally, we note that the pre-break decay slope α_2 was not influenced by our choice in break time, and the SEDs derived from these fits were only marginally influenced by the break-time choice.

4.2. The SN luminosity in the g' band

The SN light curve is best defined in the GROND r' band (3 data points), while less in i' and z' (2 data points each). In g' , it relies on only one data point (at 21 days), but this is a bright detection when compared to the expected flux of SN 1998bw at that redshift as shown by the extreme $k_{g'}$ -value. This result is remarkable, and we must note several caveats. First at all, we must note that this extreme value needs to be seen relative to SN 1998bw, which shows a strong UV damping. For example, this suppression of flux (due to the suppression of flux by metal line blanketing) was not seen in SN 2011kl (Greiner et al. 2015; Mazzali

⁴ These fits only use the g' data point at 21 d and not the upper limit at 68 d. However, the upper limit is not in disagreement with the SN 1998bw light curve shifted to $z=0.889$ (Fig. 1).

et al. 2016). A second point is that GRB/SN 140506A occurred at such a high redshift that the wavelength region in the g' band is no longer covered by the redshifted SN 1998bw $UBVRI$ data set. In other words, in order to predict the g' -band light curve, we have to extrapolate to frequencies below the U band, which is very vague. The numerical procedure we had originally developed in Zeh et al. (2004) assumes that for $\nu > \nu(U \text{ band})$ the SN flux scales $\propto \nu^{-3}$, normalized to the U -band flux. The results of this approach are given in Tables 2 and 3. In Klose et al. (2019), where we present GRB-SN data of four events between redshifts 0.4 and 0.8, it became clear, however, that this procedure potentially under-predicts the flux of a GRB-SN in this wavelength regime.

In order to improve our numerical procedure and overcome the above caveats, we modified our SN 1998bw model as follows: we adopted a pure black body radiation of the SN shell and calculated its (time-dependent) effective temperature T_{eff} based on the observed $UBVRI$ broadband photometry as it was published in Clocchiatti et al. (2011). Based on this model, with T_{eff} being a function of time, we extrapolated to the blueshifted g' -band frequencies. This approach increases the “predicted” peak brightness of SN 140506A by about 0.25 mag and makes the $k_{g'}$ value correspondingly slightly smaller (a factor ~ 1.3).

A final consideration is that the g' value is based on a single data point. We can muse as to how the luminosity would change if the transient had also been detected at 68 days in g' . The upper limit measured is significantly bluer than even the host-subtracted $g' - r'$ color measured at 21 d. We wanted to know what the luminosity would be if the SN were detected in g' at a fainter magnitude. As we have no real grasp of the color evolution, we assumed the $g' - r'$ remains constant, and we derived a g' magnitude at 68 d based on the host-subtracted r' detection and the color measured at 21 d. We then added the host-galaxy flux to the value, which ended up being 0.1 mag fainter in total than the upper limit, and redid the fit (with a break time fixed to 7 d) with the different host-galaxy magnitudes included, as before. Results for this fit are shown in the last block of Table 3. Hence, the SN has become fainter in g' (as expected), but actually slightly more luminous in the other bands; the fit is essentially unchanged in quality, $\chi^2/\text{d.o.f.} = 0.77$. The main result, however, is that the SN in g' is not much fainter than it was before (only 5%). Overall, although we consider the detection of an additional g' -component to the late-time afterglow to be real, it remains a matter of speculation how luminous the SN associated with GRB 140506A was in the blueshifted g' band.

4.3. Color evolution as evidence of an emerging SN component

Between four and 21 days, the broadband SED of the OT changed, $g' - r'$ was decreasing, and $r' - z'$ was increasing (Fig. 4). While a color evolution during the afterglow phase is not an unknown phenomenon, it is relatively rare (e.g., GRB 091127 Filgas et al. 2011, GRB 111209A Kann et al. 2018, and GRB 130427A Perley et al. 2014) and has never been observed due to pure afterglow light weeks after a burst (after correcting for an emerging host-galaxy flux). It is best understood as being due to a rising thermal component (e.g. Olivares E. et al. 2015), and thus it is a strong piece of evidence that an observed bump in an afterglow light curve represents an underlying SN component. In fact, such color evolution as evidence of an upcoming SN was already pointed out in the case of the very first cosmologically remote GRB-SN (030329/2003dh; Zeh et al. 2003).

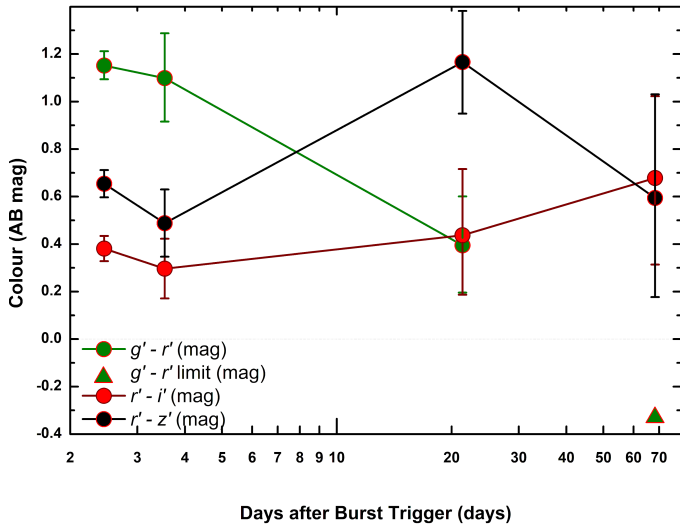


Fig. 4. Color evolution of optical transient following GRB 140506A. Data are corrected for Galactic extinction, host-galaxy-subtracted, and given in AB magnitudes. The first two epochs evolve achromatically within errors, but then a clear color change is seen after three weeks, with the transient becoming both bluer in $g' - r'$ and redder in $r' - z'$. There is likely further evolution in the last epoch at 68 d, but the transient is no longer detected in g' to a non-constraining limit, and the errors are large in the two other colors.

The $r' - z'$ color of the OT (roughly corresponding to an $U - g'$ color in the GRB rest frame) increases up to 1 mag at 21 days (i.e., at 11.6 days rest-frame time). Also, the $g' - r'$ color evolution (roughly corresponding to the rest-frame $uvw1 - u$) at 21 days supports a similar evolution, though this is based on a single detection. Such colors of $U - g' \sim 1-2$ mags have already been observed between ten and 20 days in other GRB-SNe including GRB-SN 120422A-SN2012bz, 130427A-SN2013cq, and 171205A-SN2017iuk (e.g., Schulze et al. 2014; Becerra et al. 2017; Izzo et al. 2019) and GRB-SN 081007-2008hw, 091127-2009nz, 101219B-2010ma (Olivares E. et al. 2015) and GRB 130831A (associated with a bump-only SN; Klose et al. 2019). The last three events were all at a redshift $z \sim 0.5$, and thus their $g' - i'$ color corresponded to the $r' - z'$ of GRB 140506A. The OT that followed GRB 111209A showed a similar color of 1 mag at $\sim 1-13$ days (rest-frame time) when we consider its absolute magnitudes at 2735 and 4556 Å (Table 2 in Kann et al. 2019). In other words, the observed color evolution of the OT following GRB 140506A is a strong indicator of an emerging SN component.

We note that the observed color change could suggest a late-time contribution from the interaction of the SN ejecta with circumstellar material (CSM). CSM interaction can manifest itself through discrete emission lines, as seen in SNe IIn (Smith 2017), but also through a blue pseudo-continuum, similar to that seen in SNe Ia-CSM, Ibn, Icn, and some SNe IIn (e.g., Silverman et al. 2013; Hosseinzadeh et al. 2017; Gal-Yam et al. 2022; Perley et al. 2022). There is also a small but growing number of SNe Ic-BL with evidence of late-time CSM interaction, such as SN 2017ens (Chen et al. 2018) and SN 2023xxf (Kuncarayakti et al. 2023). To further explore this color-change in GRB-SNe, we need to collect more observations in the rest-frame UV. This can be done by observing rare nearby events in the UV, or with deep optical observations of the more distant GRB-SNe.

4.4. The missing spectroscopic confirmation of the SN

Spectra of the optical transient following GRB 140506A were obtained by Fynbo et al. (2014) at 8.8 h, 33 h, and 52 d post burst. They call the spectrum taken at 52 days a host-galaxy spectrum. However, our data show that it was actually taken during the SN phase (which was not recognized by these authors). This spectrum covers the wavelength range of 660 – 977 nm; that is, it is missing the blue part that might show SN features (which, e.g., were covered in the X-shooter spectrum of GRB 111209A-SN 2011kl; Greiner et al. 2015; Mazzali et al. 2016). Furthermore, the spectrum is of low S/N, and only a host-galaxy emission line is detected. Therefore, while it is a spectrum taken during the SN, it cannot count as an actual SN spectrum. Consequently, the SN following GRB 140506A is bump-only, with only category D evidence following the characterization of Hjorth & Bloom (2012).⁵

4.5. GRB-SN 140506A compared with GRB 111209A-SN 2011kl

The luminosity factors of the supernova shown in the right part of Table 2 are extreme, and significantly larger than those of even SN 2011kl, the SN associated with GRB 111209A (Kann et al. 2019). We note that this GRB had a somewhat lower redshift ($z = 0.67702$, Kann et al. 2018), and therefore the observer-frame bands (which are identical) are not the same in the rest frame compared to GRB 140506A. The observer-frame z' band of GRB 140506A roughly agrees with the observer-frame i' band for GRB 111209A, both being close to the rest-frame $B - g'$ band (where the SN 1998bw template is also well defined). In this case, it is $k_{z'}^{\text{GRB-SN 140506A}} = 3.32 \pm 1.45$ versus $k_{i'}^{\text{SN 2011kl}} = 1.81 \pm 0.22$. Therefore, the SN associated with GRB 140506A is the most luminous detected so far. However, the error bars are large, and the difference is only slightly above 1σ . In the case of GRB 140506A, the extinction is clearly very large (Fynbo et al. 2014; Heintz et al. 2017, and Sect. 3.3), which is in contrast with the (relatively small) extinction measured from the GRB 111209A afterglow (Kann et al. 2018, 2019).

We also note that the X-ray light curve shows a deviation from a pure single power-law decay downward at about 6–7 d, that we explain as the possible jet break. However, the flux has recovered by 14 d, and the further decay is in agreement with the earlier afterglow decay. Such an evolution is very similar to the atypical X-ray light curve of GRB 111209A. Kann et al. (2019) speculated this might be a jet break (which is detected in the UV-optical for GRB 111209A) combined with rising X-ray emission associated with SN 2011kl. A similar phenomenon may be visible here, associated with the extremely luminous and blue SN. However, the sparse data mean this remains speculation.

4.6. The GRB-SN luminosity-stretch diagram

There has been discussion on the use of GRB-SNe as standard candles, with an initial study done by Schulze et al. (2014, their figure 11), and expanded upon by Cano (2014); Cano & Jakobsen (2014); Li & Hjorth (2014); Li et al. (2014). To place the SN of GRB 140506A into such a context, we collected data from the samples of Ferrero et al. (2006), Thöne et al. (2011), and Klose et al. (2019) and use, similarly to Schulze et al. (2014), a “quasi

⁵ A bump, but the inferred SN properties are not fully consistent with other GRB-SNe, or the bump was not well sampled, or there is no spectroscopic redshift of the GRB. (Hjorth & Bloom 2012)

Table 3. Alternative solution for GRB 140506A supernova component.

| Fit model | s | k (fitted) | k (extinction-corrected) |
|-----------------|-----------------|--------------------------|----------------------------|
| 12 day break | 1.97 ± 0.11 | $k_{g'} = 5.69 \pm 1.17$ | $k_{g'} = 80.45 \pm 20.80$ |
| | | $k_{r'} = 1.42 \pm 0.34$ | $k_{r'} = 7.92 \pm 2.27$ |
| | | $k_{i'} = 1.35 \pm 0.37$ | $k_{i'} = 5.58 \pm 1.75$ |
| | | $k_{z'} = 1.12 \pm 0.39$ | $k_{z'} = 3.72 \pm 1.40$ |
| 7 day break | 1.91 ± 0.12 | $k_{g'} = 5.17 \pm 1.23$ | $k_{g'} = 73.11 \pm 20.80$ |
| Two g' points | | $k_{r'} = 1.23 \pm 0.40$ | $k_{r'} = 6.86 \pm 2.50$ |
| | | $k_{i'} = 1.25 \pm 0.41$ | $k_{i'} = 5.14 \pm 1.88$ |
| | | $k_{z'} = 1.04 \pm 0.42$ | $k_{z'} = 3.46 \pm 1.49$ |

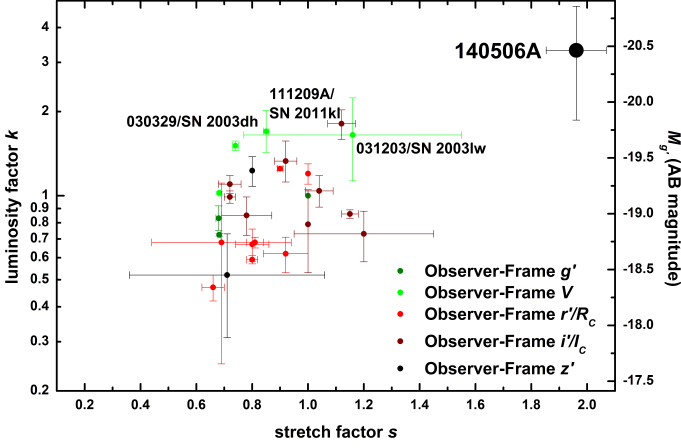


Fig. 5. Luminosity of GRB-SNe (given in luminosity versus the luminosity of an SN 1998bw template, k) versus their peak time (given in stretch versus the light curve of an SN 1998bw template, s). SN 1998bw is per definitionem at $(k, s) = (1, 1)$. These (k, s) values are derived from observer-frame filter fits given in the legend (and color-coded), which are close to the rest-frame g' filter; hence, they are all roughly comparable. The right-hand scale in absolute magnitude is therefore not completely precise. We highlight several luminous GRB-SNe. The SN bump associated with GRB 140506A stands out strongly but represents an extension of the luminosity-duration correlation that has been discussed in the literature (e.g., Schulze et al. 2014; Cano et al. 2017; Klose et al. 2019).

rest-frame g' band”, using (k, s) values where the observer-frame band corresponds reasonably to the rest-frame g' band. This is an imprecise process, but it is sufficient to yield a qualitative result. We show the resulting data in Fig. 5. We color-code the observer-frame bands in which the SNe were fit, which acts as a rough redshift measure.

Figure 5 shows that the GRB 140506A supernova is a strong outlier compared to the other GRB-SNe, even GRB 111209A-SN 2011kl, both being far more luminous and far slower in terms of light-curve evolution. However, the combination of these two extremes places the GRB 140506A-SN on the extension of the GRB-SN Phillips relation first discussed by Schulze et al. (2014). A more quantitative analysis will be performed in future work. In Fig. 5, we also show the absolute magnitude in g' on the right y axis. We took the M_B of SN 1998bw, corrected it for host-galaxy extinction (Kann et al. 2019), and estimated $B - g'$ (SN 1998bw) = 0.2 mag. We note the data points do not agree with this scale exactly, as they are only close to the rest-frame g' band.

4.7. Dust destruction and color evolution

Fynbo et al. (2014) reported on a small but definite shift in the location of the steep flux depression from their first to their second spectrum. We cannot check for a respective color change as there is no multicolor photometry during the first epoch. Heintz et al. (2017) pointed out that this effect may be linked to the emission region in the second epoch being significantly larger. The very high collimation of GRB afterglows at very early times implies that if dust destruction were to be induced in a dust curtain near the GRB, the affected area would be significantly smaller than the emission region at later times. Morgan et al. (2014) reported the signature of dust destruction in the very early afterglow of GRB 120119A; however, even after the extinction becomes constant, it is still very high, $A_V \approx 1.1$ mag (Morgan et al. 2014; Japelj et al. 2015; Zafar et al. 2018b, Kann et al., in prep.), similar to our result for GRB 140506A. The color evolution induced by dust burning is only detected in the first ≈ 100 rest-frame seconds, however, in the case of GRB 120119A. At such times, the only data we have for GRB 140506A are the unfiltered UVOT *white* data beginning 56 rest-frame s post-trigger (though, we note the existence of several further strong X-ray flares in Fig. 1). While these few data points do not show a flatter evolution or even rise (emergence from a dusty envelope was a model suggested for the light-curve behavior of GRB 030418, Rykoff et al. 2004), the lack of any color evolution does not allow us to set any constraints on the potential existence of dust burning, or lack thereof.

5. Conclusions

We studied the light curve, afterglow SED, and potential SN of the ordinary GRB 140506A, which so far had only been remarkable for its high line-of-sight extinction, peculiar dust law, and spectral features (Fynbo et al. 2014; Heintz et al. 2017). We find that despite clear strong reddening, the afterglow is detected all the way into the UV at early times, allowing us to create a broadband SED that confirms the high extinction and favors an MW-type extinction law with a clear 2175 Å bump.

The late-time transient shows a clear color change and a long plateau phase before reaching a fainter host-galaxy level, which we interpret as the SN following GRB 140506A. This is a remarkable result, especially the strong detection in the observer-frame g' band, considering the high redshift of $z \approx 0.9$ (the highest redshift at which GRB-SNe have been detected so far is $z \approx 1$, Della Valle et al. 2003; Masetti et al. 2005). It becomes even more remarkable once the strong extinction is corrected for, resulting in the most luminous (but also most slowly evolving) GRB-SN detected so far. The SN remained luminous

deep into the UV, similar to GRB 111209A-SN 2011kl. The latter event was, however, associated with a remarkable, ultra-long GRB (Gendre et al. 2013; Greiner et al. 2015; Mazzali et al. 2016; Kann et al. 2018, 2019), whereas GRB 140506A is unremarkable in terms of both duration and energetics.

The very luminous but also very slowly evolving SN of GRB 140506A hints that a luminosity-peak time correlation for GRB-SNe, which would have implications for cosmological measurements, exists and extends all the way into a part of the parameter space that has so far not been populated. It makes it clear that late-time follow-up of GRB afterglows at $z \lesssim 1$ can always yield interesting surprises (unless the host galaxy is too bright and masks the SN emission, which can happen even at significantly lower redshifts as in the case of the faint SN accompanying XRF 100418A, Niino et al. 2012; de Ugarte Postigo et al. 2018). More overly luminous SNe such as the one associated with GRB 140506A need to be found to allow the use of GRB-SNe as robust cosmological tracers.

Acknowledgements. The co-authors wish to thank the editor for allowing us to complete this study after the recent loss of our colleague David Alexander Kann, R.I.P. 10. 03. 2023. We thank the referee for the very valuable report which helped improve the clarity of the paper. We also thank S. Schmidl for help with the figures. DAK acknowledges support from Spanish National Research Project RTI2018-098104-J-I00 (GRBPhot). AdUP and CCT acknowledge support from Ramón y Cajal fellowships RyC-2012-09975 and RyC-2012-09984 and the Spanish Ministry of Economy and Competitiveness through projects AYA2014-58381-P and AYA2017-89384-P, AdUP furthermore from the BBVA foundation. AR acknowledge support from PRIN-MIUR 2017 (grant 20179ZF5KS). SK acknowledges support by the Thüringer Ministerium für Bildung, Wissenschaft und Kultur under FKZ 12010-514 and by grants DFG KI 766/16-1 and 766/16-3. SS is supported by LBNL Subcontract NO. 7707915. This work made use of data supplied by the UK Swift Science Data Centre at the University of Leicester.

References

Agüí Fernández, J. F., Thöne, C. C., Kann, D. A., et al. 2023, *MNRAS*, 520, 613
 Ahumada, T., Singer, L. P., Anand, S., et al. 2021, *Nature Astronomy*, 5, 917
 Becerra, R. L., Watson, A. M., Lee, W. H., et al. 2017, *ApJ*, 837, 116
 Breeveld, A. A., Landsman, W., Holland, S. T., et al. 2011, in *American Institute of Physics Conference Series*, Vol. 1358, American Institute of Physics Conference Series, ed. J. E. McEnery, J. L. Racusin, & N. Gehrels, 373–376
 Burrows, D. N., Hill, J. E., Nousek, J. A., et al. 2005, *Space Sci. Rev.*, 120, 165
 Cano, Z. 2014, *ApJ*, 794, 121
 Cano, Z. & Jakobsson, P. 2014, *MNRAS*, submitted (arXiv:1409.3570) [arXiv:1409.3570]
 Cano, Z., Wang, S.-Q., Dai, Z.-G., & Wu, X.-F. 2017, *Advances in Astronomy*, 2017, 8929054
 Cardelli, J. A., Clayton, G. C., & Mathis, J. S. 1989, *ApJ*, 345, 245
 Chen, T.-W., Inserra, C., Fraser, M., et al. 2018, *ApJ*, 867, L31
 Clocchiatti, A., Suntzeff, N. B., Covarrubias, R., & Candia, P. 2011, *AJ*, 141, 163
 de Ugarte Postigo, A., Thöne, C. C., Bensch, K., et al. 2018, *A&A*, 620, A190
 Della Valle, M., Malesani, D., Benetti, S., et al. 2003, *A&A*, 406, L33
 Elíasdóttir, Á., Fynbo, J. P. U., Hjorth, J., et al. 2009, *ApJ*, 697, 1725
 Evans, P. A., Beardmore, A. P., Page, K. L., et al. 2009, *MNRAS*, 397, 1177
 Evans, P. A., Beardmore, A. P., Page, K. L., et al. 2007, *A&A*, 469, 379
 Ferrero, P., Kann, D. A., Zeh, A., et al. 2006, *A&A*, 457, 857
 Filgas, R., Greiner, J., Schady, P., et al. 2011, *A&A*, 535, A57
 Fitzpatrick, E. L. & Massa, D. 2007, *ApJ*, 663, 320
 Fynbo, J. P. U., Krühler, T., Leighly, K., et al. 2014, *A&A*, 572, A12
 Gal-Yam, A., Bruch, R., Schulze, S., et al. 2022, *Nature*, 601, 201
 Galama, T. J., Vreeswijk, P. M., van Paradijs, J., et al. 1998, *Nature*, 395, 670
 Gehrels, N., Chincarini, G., Giommi, P., et al. 2004, *ApJ*, 611, 1005
 Gendre, B., Stratta, G., Atteia, J. L., et al. 2013, *ApJ*, 766, 30
 Golenetskii, S., Aptekar, R., Frederiks, D., et al. 2014, GRB Coordinates Network, 16223
 Golenetskii, S., Aptekar, R., Mazets, E., et al. 2011, GCN Circulars, 12663
 Gompertz, B. P., Burrows, D. N., Cenko, S. B., et al. 2014, GRB Coordinates Network, 16214
 Greiner, J., Mazzali, P. A., Kann, D. A., et al. 2015, *Nature*, 523, 189
 Heintz, K. E., Fynbo, J. P. U., Jakobsson, P., et al. 2017, *A&A*, 601, A83
 Hjorth, J. & Bloom, J. S. 2012, *The Gamma-Ray Burst - Supernova Connection*, 169–190

Hjorth, J., Sollerman, J., Møller, P., et al. 2003, *Nature*, 423, 847
 Hosseinzadeh, G., Arcavi, I., Valenti, S., et al. 2017, *ApJ*, 836, 158
 Izzo, L., de Ugarte Postigo, A., Maeda, K., et al. 2019, *Nature*, 565, 324
 Japelj, J., Covino, S., Gomboc, A., et al. 2015, *A&A*, 579, A74
 Jenke, P. 2014, GRB Coordinates Network, 16220
 Kann, D. A., Klose, S., Zhang, B., et al. 2011, *ApJ*, 734, 96
 Kann, D. A., Klose, S., Zhang, B., et al. 2010, *ApJ*, 720, 1513
 Kann, D. A., Schady, P., Olivares, E. F., et al. 2018, *A&A*, 617, A122
 Kann, D. A., Schady, P., Olivares, E. F., et al. 2019, *A&A*, 624, A143
 Klose, S., Schmidl, S., Kann, D. A., et al. 2019, *A&A*, 622, A138
 Krühler, T., Küpcü Yoldaş, A., Greiner, J., et al. 2008, *ApJ*, 685, 376
 Kuncarayakti, H., Sollerman, J., Izzo, L., et al. 2023, *A&A*, 678, A209
 Levan, A. J., Tanvir, N. R., Starling, R. L. C., et al. 2014, *ApJ*, 781, 13
 Li, X. & Hjorth, J. 2014, *A&A*, submitted (arXiv:1407.3506) [arXiv:1407.3506]
 Li, X., Hjorth, J., & Wojtak, R. 2014, *ApJ*, 796, L4
 Markwardt, C. B., Barthelmy, S. D., Baumgartner, W. H., et al. 2014, GRB Coordinates Network, 16218
 Masetti, N., Palazzi, E., Pian, E., et al. 2005, *A&A*, 438, 841
 Matheson, T., Garnavich, P. M., Stanek, K. Z., et al. 2003, *ApJ*, 599, 394
 Mazzali, P. A., Deng, J., Nomoto, K., et al. 2006, *Nature*, 442, 1018
 Mazzali, P. A., Sullivan, M., Pian, E., Greiner, J., & Kann, D. A. 2016, *MNRAS*, 458, 3455
 Melandri, A., Pian, E., D’Elia, V., et al. 2014, *A&A*, 567, A29
 Morgan, A. N., Perley, D. A., Cenko, S. B., et al. 2014, *MNRAS*, 440, 1810
 Niino, Y., Hashimoto, T., Aoki, K., et al. 2012, *PASJ*, 64, 115
 Oates, S. R., Page, M. J., Schady, P., et al. 2009, *MNRAS*, 395, 490
 Olivares, E. F., Greiner, J., Schady, P., et al. 2015, *A&A*, 577, A44
 Pei, Y. C. 1992, *ApJ*, 395, 130
 Perley, D. A., Cenko, S. B., Corsi, A., et al. 2014, *ApJ*, 781, 37
 Perley, D. A., Sollerman, J., Schulze, S., et al. 2022, *ApJ*, 927, 180
 Pian, E., Mazzali, P. A., Masetti, N., et al. 2006, *Nature*, 442, 1011
 Poole, T. S., Breeveld, A. A., Page, M. J., et al. 2008, *MNRAS*, 383, 627
 Roming, P. W. A., Kennedy, T. E., Mason, K. O., et al. 2005, *Space Sci. Rev.*, 120, 95
 Rossi, A., Rothberg, B., Palazzi, E., et al. 2022, *ApJ*, 932, 1
 Rykoff, E. S., Smith, D. A., Price, P. A., et al. 2004, *ApJ*, 601, 1013
 Schlafly, E. F. & Finkbeiner, D. P. 2011, *ApJ*, 737, 103
 Schulze, S., Malesani, D., Cucchiara, A., et al. 2014, *A&A*, 566, A102
 Siegel, M. H. & Gompertz, B. P. 2014, GRB Coordinates Network, 16219
 Silverman, J. M., Nugent, P. E., Gal-Yam, A., et al. 2013, *ApJS*, 207, 3
 Smith, N. 2017, in *Handbook of Supernovae*, ed. A. W. Alsabti & P. Murdin, 403
 Spergel, D. N., Verde, L., Peiris, H. V., et al. 2003, *ApJS*, 148, 175
 Stanek, K. Z., Matheson, T., Garnavich, P. M., et al. 2003, *ApJ*, 591, L17
 Stratta, G., Gendre, B., Atteia, J. L., et al. 2013, *ApJ*, 779, 66
 Thöne, C. C., de Ugarte Postigo, A., Fryer, C. L., et al. 2011, *Nature*, 480, 72
 Tsvetkova, A., Frederiks, D., Golenetskii, S., et al. 2017, *ApJ*, 850, 161
 Woosley, S. E. & Bloom, J. S. 2006, *ARA&A*, 44, 507
 Xu, D., de Ugarte Postigo, A., Leloudas, G., et al. 2013, *ApJ*, 776, 98
 Zafar, T., Heintz, K. E., Fynbo, J. P. U., et al. 2018a, *ApJ*, 860, L21
 Zafar, T., Watson, D., Elíasdóttir, Á., et al. 2012, *ApJ*, 753, 82
 Zafar, T., Watson, D., Møller, P., et al. 2018b, *MNRAS*, 479, 1542
 Zeh, A., Klose, S., & Greiner, J. 2003, GRB Coordinates Network, 2081, 1
 Zeh, A., Klose, S., & Hartmann, D. H. 2004, *ApJ*, 609, 952
 Zhang, B., Zhang, B.-B., Virgili, F. J., et al. 2009, *ApJ*, 703, 1696
 Zhang, B. B., Liu, Z. K., Peng, Z. K., et al. 2021, *Nature Astronomy*, 5, 911

Appendix A: Additional observational data

Table A.1. UVOT observations of GRB 140506A.

| Δt (days) | mag | filter |
|-------------------|----------------------------|---------|
| 0.007419 | $21.334^{+2.296}_{-0.685}$ | uvw2 |
| 0.009423 | $21.434^{+4.156}_{-0.741}$ | uvw2 |
| 0.012113 | $21.153^{+2.116}_{-0.672}$ | uvw2 |
| 0.014116 | $21.462^{+4.645}_{-0.745}$ | uvw2 |
| 0.073942 | $22.928^{+1.628}_{-0.624}$ | uvw2 |
| 0.016118 | > 20.447 | uvw2 UL |
| 0.018121 | > 20.991 | uvw2 UL |
| 0.195006 | > 23.420 | uvw2 UL |
| 0.535097 | > 23.400 | uvw2 UL |
| 0.795653 | > 22.917 | uvw2 UL |
| 5.834459 | > 24.823 | uvw2 UL |
| 13.803396 | > 23.589 | uvw2 UL |
| 17.937837 | > 23.488 | uvw2 UL |
| 0.007986 | $20.189^{+0.912}_{-0.489}$ | uvm2 |
| 0.012679 | $20.731^{+1.594}_{-0.620}$ | uvm2 |
| 0.078682 | $21.707^{+0.623}_{-0.393}$ | uvm2 |
| 0.009999 | > 19.788 | uvm2 UL |
| 0.014680 | > 20.153 | uvm2 UL |
| 0.016684 | > 19.684 | uvm2 UL |
| 0.062059 | > 21.734 | uvm2 UL |
| 0.340650 | > 22.883 | uvm2 UL |
| 2.361840 | > 23.194 | uvm2 UL |
| 2.529452 | > 22.703 | uvm2 UL |
| 6.797721 | > 22.957 | uvm2 UL |
| 10.725055 | > 23.950 | uvm2 UL |
| 18.395811 | > 24.251 | uvm2 UL |
| 22.595256 | > 23.429 | uvm2 UL |
| 26.761876 | > 23.785 | uvm2 UL |
| 30.580328 | > 24.084 | uvm2 UL |
| 0.008277 | $19.318^{+0.468}_{-0.326}$ | uvw1 |
| 0.012966 | $20.678^{+1.647}_{-0.626}$ | uvw1 |
| 0.016978 | $20.198^{+0.994}_{-0.510}$ | uvw1 |
| 0.064437 | $22.190^{+0.862}_{-0.474}$ | uvw1 |
| 0.081058 | $22.188^{+1.442}_{-0.598}$ | uvw1 |
| 0.014971 | > 20.073 | uvw1 UL |
| 0.348816 | > 21.957 | uvw1 UL |
| 0.465948 | > 22.813 | uvw1 UL |
| 0.734638 | > 23.819 | uvw1 UL |
| 3.201317 | > 23.158 | uvw1 UL |
| 7.797540 | > 23.376 | uvw1 UL |

Table A.1. continued.

| Δt (days) | mag | filter |
|-------------------|--|-----------------|
| 11.663524 | > 24.137 | <i>uvw</i> 1 UL |
| 15.791810 | > 24.423 | <i>uvw</i> 1 UL |
| 0.003941 | 17.923 ^{+0.131} _{-0.117} | <i>u</i> |
| 0.004288 | 17.838 ^{+0.124} _{-0.111} | <i>u</i> |
| 0.004691 | 18.555 ^{+0.166} _{-0.144} | <i>u</i> |
| 0.005154 | 18.484 ^{+0.160} _{-0.140} | <i>u</i> |
| 0.005618 | 18.884 ^{+0.212} _{-0.177} | <i>u</i> |
| 0.006137 | 18.763 ^{+0.178} _{-0.153} | <i>u</i> |
| 0.006546 | 18.657 ^{+0.278} _{-0.221} | <i>u</i> |
| 0.008560 | 18.816 ^{+0.352} _{-0.265} | <i>u</i> |
| 0.013254 | 19.328 ^{+0.753} _{-0.440} | <i>u</i> |
| 0.015102 | 19.580 ^{+0.303} _{-0.237} | <i>u</i> |
| 0.017261 | 19.820 ^{+2.739} _{-0.708} | <i>u</i> |
| 0.066808 | 20.631 ^{+0.260} _{-0.210} | <i>u</i> |
| 0.083428 | > 20.218 | <i>u</i> UL |
| 0.400859 | > 24.178 | <i>u</i> UL |
| 0.484796 | > 19.811 | <i>u</i> UL |
| 0.743324 | > 21.479 | <i>u</i> UL |
| 4.798999 | > 22.811 | <i>u</i> UL |
| 8.223336 | > 23.195 | <i>u</i> UL |
| 20.363598 | > 22.264 | <i>u</i> UL |
| 24.395194 | > 23.851 | <i>u</i> UL |
| 28.659326 | > 23.269 | <i>u</i> UL |
| 0.006843 | 19.346 ^{+1.227} _{-0.561} | <i>b</i> |
| 0.008847 | 19.083 ^{+1.174} _{-0.551} | <i>b</i> |
| 0.015394 | 19.763 ^{+0.801} _{-0.456} | <i>b</i> |
| 0.017547 | 19.533 ^{+2.869} _{-0.713} | <i>b</i> |
| 0.069184 | 20.504 ^{+0.438} _{-0.311} | <i>b</i> |
| 0.130621 | 21.261 ^{+0.370} _{-0.275} | <i>b</i> |
| 0.013540 | > 18.433 | <i>b</i> UL |
| 0.084803 | > 18.798 | <i>b</i> UL |
| 0.411421 | > 22.854 | <i>b</i> UL |
| 0.663690 | > 21.600 | <i>b</i> UL |
| 0.001132 | 17.034 ^{+0.310} _{-0.241} | <i>v</i> |
| 0.007704 | 18.110 ^{+0.536} _{-0.357} | <i>v</i> |
| 0.012396 | 17.866 ^{+0.527} _{-0.353} | <i>v</i> |
| 0.016400 | 18.182 ^{+0.803} _{-0.457} | <i>v</i> |
| 0.059688 | 20.106 ^{+0.518} _{-0.349} | <i>v</i> |
| 0.076311 | 19.881 ^{+0.543} _{-0.360} | <i>v</i> |
| 0.009704 | > 18.423 | <i>v</i> UL |
| 0.014398 | > 17.990 | <i>v</i> UL |
| 0.330130 | > 20.637 | <i>v</i> UL |

Table A.1. continued.

| Δt (days) | mag | filter |
|-------------------|--|----------|
| 0.592875 | > 20.325 | v UL |
| 0.802144 | > 20.476 | v UL |
| 0.001360 | 17.676 ^{+0.084} _{-0.078} | white |
| 0.001476 | 17.928 ^{+0.096} _{-0.088} | white |
| 0.001591 | 17.949 ^{+0.097} _{-0.089} | white |
| 0.001707 | 17.943 ^{+0.096} _{-0.088} | white |
| 0.001823 | 17.835 ^{+0.090} _{-0.083} | white |
| 0.001939 | 18.115 ^{+0.105} _{-0.096} | white |
| 0.002055 | 18.058 ^{+0.101} _{-0.093} | white |
| 0.002170 | 18.115 ^{+0.105} _{-0.096} | white |
| 0.002286 | 18.212 ^{+0.110} _{-0.100} | white |
| 0.002458 | 18.279 ^{+0.080} _{-0.075} | white |
| 0.002689 | 18.281 ^{+0.080} _{-0.074} | white |
| 0.002920 | 18.311 ^{+0.082} _{-0.076} | white |
| 0.007126 | 19.255 ^{+0.160} _{-0.139} | white |
| 0.009129 | 19.735 ^{+0.275} _{-0.219} | white |
| 0.011030 | 19.916 ^{+0.115} _{-0.104} | white |
| 0.013822 | 19.986 ^{+0.410} _{-0.297} | white |
| 0.015823 | 20.398 ^{+0.720} _{-0.429} | white |
| 0.017829 | 20.103 ^{+0.556} _{-0.366} | white |
| 0.071559 | 20.909 ^{+0.160} _{-0.140} | white |
| 0.141189 | 22.429 ^{+0.265} _{-0.213} | white |
| 1.806576 | 23.528 ^{+0.717} _{-0.428} | white |
| 0.417553 | > 21.972 | white UL |
| 0.672448 | > 24.344 | white UL |
| 0.966973 | > 24.512 | white UL |
| 1.265749 | > 23.492 | white UL |
| 1.468435 | > 24.223 | white UL |
| 1.976269 | > 23.667 | white UL |

Notes. All data are in AB magnitudes and not corrected for Galactic foreground extinction. Midtimes were derived with the geometric mean of start and stop times. $t = \sqrt{(t_1 - t_0)(t_2 - t_0)}$, hereby $t_{1,2}$ are the absolute start and stop times, and t_0 is the *Swift* trigger time. To obtain Vega magnitudes, it is $uvw2_{AB} - uvw2_{Vega} = 1.73$ mag, $uvm2_{AB} - uvm2_{Vega} = 1.69$ mag, $uvw1_{AB} - uvw1_{Vega} = 1.51$ mag, $u_{AB} - u_{Vega} = 1.02$ mag, $b_{AB} - b_{Vega} = -0.13$ mag, $v_{AB} - v_{Vega} = -0.01$ mag, and $white_{AB} - white_{Vega} = 0.80$ mag (as given at http://swift.gsfc.nasa.gov/analysis/uvot_digest/zeropts.html). Corrections for Galactic extinction are, using $E_{(B-V)} = 0.080$ mag (Schlafly & Finkbeiner 2011) and the Galactic extinction curve of Cardelli et al. (1989): $A_{uvw2} = 0.728$ mag, $A_{uvm2} = 0.763$ mag, $A_{uvw1} = 0.539$ mag, $A_u = 0.405$ mag, $A_b = 0.328$ mag, $A_v = 0.256$ mag, and $A_{white} = 0.397$ mag.